



**CHALMERS**  
UNIVERSITY OF TECHNOLOGY

## Required and received SNRs in coded modulation

Downloaded from: <https://research.chalmers.se>, 2025-06-18 04:22 UTC

Citation for the original published paper (version of record):

Yoshida, T., Igarashi, K., Binkai, M. et al (2020). Required and received SNRs in coded modulation. European Conference on Optical Communication, ECOC.  
<http://dx.doi.org/10.1109/ECOC48923.2020.9333308>

N.B. When citing this work, cite the original published paper.

# Required and Received SNRs in Coded Modulation

Tsuyoshi Yoshida<sup>(1,2)</sup>, Koji Igarashi<sup>(2)</sup>, Masashi Binkai<sup>(1)</sup>, Shun Chikamori<sup>(1)</sup>, Mikael Mazur<sup>(3)</sup>, Jochen Schröder<sup>(3)</sup>, Keisuke Matsuda<sup>(1)</sup>, Shota Koshikawa<sup>(1)</sup>, Naoki Suzuki<sup>(1)</sup>, Magnus Karlsson<sup>(3)</sup>, and Erik Agrell<sup>(3)</sup>

<sup>(1)</sup> IT R&D Center, Mitsubishi Electric Corporation, Yoshida.Tsuyoshi@ah.MitsubishiElectric.co.jp

<sup>(2)</sup> Graduate School of Engineering, Osaka University

<sup>(3)</sup> Fiber Optic Communications Research Center, Chalmers University of Technology

**Abstract** Coded modulation techniques aim at reducing the required signal-to-noise ratio (SNR) over the Gaussian channel with an average energy constraint; however, such techniques tend to degrade the received SNR. We studied the balance of required and received SNRs for a realistic system design.

## Introduction

Coded modulation<sup>[1-8]</sup> is one of the key technologies in optical fiber communication to realize better tradeoffs between performance and complexity. Forward error correction (FEC) efficiently eliminates bit errors, multilevel modulation controls spectral efficiency, and constellation shaping reduces the gap between the Shannon capacity and achievable rates for pragmatic modulation formats with uniformly distributed symbol probabilities.

Coded modulation is mainly studied for a small *required* signal-to-noise ratio (SNR) at a certain spectral efficiency (SE) and given hardware resources. Coded modulation techniques such as geometric/probabilistic shaping<sup>[1,2,4-7]</sup> with an FEC often use formats with a larger number of signal points, a larger peak-to-average power ratio (PAPR), and a larger kurtosis. These characteristics will not cause performance degradation over an ideal Gaussian channel with an average energy constraint. However, they may lead to a smaller *received* SNR<sup>[9]</sup> in practice due to limitations of the effective number of bits in digital-to-analog or analog-to-digital conversion (DAC/ADC), nonlinearity in analog devices such as the Mach-Zehnder modulator and its driver, and nonideal algorithms with finite precision in the digital signal processing (DSP).

True performance improvement in deployable systems is realized if and only if the reduction in the *required* SNR is larger than the one in the *received* SNR. Thus, in this work we analyze the behaviour of such SNRs from experimental data for several modulation/shaping cases. This characterization is useful for modelling the performance of coded modulation transceivers. We also compare the required optical SNR (ROSNR) and transceiver SNR assuming bit-interleaved coded modulation (BICM)<sup>[3]</sup> or multilevel coding (MLC)<sup>[8]</sup> to find a good solution for deployable systems.

## Definition of SNRs

In systems with many optical amplifiers, the

dominant noise source is amplified spontaneous emission (ASE) from optical amplifiers. Here a Gaussian channel with an average energy constraint is assumed. Thus the system budget tends to be expressed in OSNR. In this work we set a noise bandwidth for the OSNR definition to the Nyquist limit, i.e., the symbol rate. On the other hand, the system performance is also influenced by the optical transceiver (including DSP). Modelling the transceiver imperfections as additive Gaussian noise<sup>[10]</sup> with a normalized variance  $\sigma_{\text{TR}}^2$ , the total received noise variance is

$$\sigma_{\text{eff}}^2 = \sigma_{\text{ASE}}^2 + \sigma_{\text{TR}}^2, \quad (1)$$

where  $\sigma_{\text{ASE}}^2$  equals  $1/\text{SNR}_{\text{ASE}}$  and we neglect noise from fiber nonlinearity and the other impairments. Here we define the effective received SNR as  $\text{SNR}_{\text{eff}} = 1/\sigma_{\text{eff}}^2$  and the transceiver SNR as  $\text{SNR}_{\text{TR}} = 1/\sigma_{\text{TR}}^2$ . The OSNR  $\text{SNR}_{\text{ASE}}$  can be measured from the optical spectrum, and  $\text{SNR}_{\text{eff}}$  is inversely estimated from the obtained performance such as mutual information (MI), generalized MI (GMI)<sup>[11]</sup>, normalized GMI<sup>[7]</sup>, asymmetric information (ASI)<sup>[12,13]</sup>, or uncertainty<sup>[6]</sup>. The transceiver SNR  $\text{SNR}_{\text{TR}}$  is derived from (1) based on  $\text{SNR}_{\text{ASE}}$  and  $\text{SNR}_{\text{eff}}$ . Fig. 1 shows  $\Delta\text{SNR}$  as a function of  $\text{SNR}_{\text{ASE}}$  for different  $\text{SNR}_{\text{TR}}$ , where  $\Delta\text{SNR}$  denotes SNR degradation defined by  $\text{SNR}_{\text{ASE}}/\text{SNR}_{\text{eff}}$ . For  $\text{SNR}_{\text{ASE}}$  close to  $\text{SNR}_{\text{TR}}$ ,  $\Delta\text{SNR}$  becomes significant. Note that  $\text{SNR}_{\text{TR}}$  typically ranges from 14 to 21 dB in high baud rate cases<sup>[9]</sup>. Moreover,

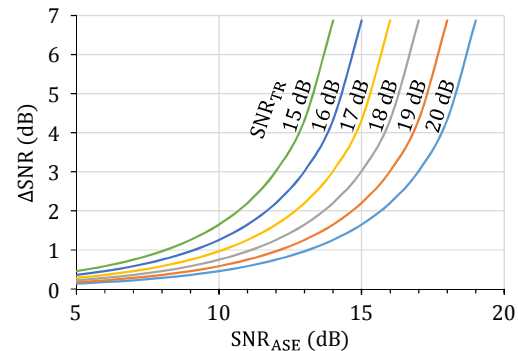


Fig. 1: Degradation of effective SNRs characterized by transceiver SNRs.

$\text{SNR}_{\text{TR}}$  is not independent of  $\text{SNR}_{\text{ASE}}$  in practice because DSP parts such as the equalizer and carrier recovery become unstable in the low OSNR regime.

### Experimental conditions

We investigate the SNR performance by offline experiments with a setup, which is almost the same as the one in Ref.<sup>[14]</sup>. In this work, we performed noise loading experiments only. The symbol rate was 24 Gsymbol/s and the signal was shaped with a 1% roll-off root-raised cosine filter. The linewidths of the transmitter and local oscillator lasers were 100 kHz. The receiver side DSP, which consisted of adaptive equalization and carrier recovery, was fully pilot-aided<sup>[15]</sup>, enabling constellation-independent processing. The pilot signal was quadrature phase-shift keyed (QPSK), the insertion ratio was < 4%, and pilots and data had the same average symbol energy. Each captured data set consisted of  $\sim 10^5$  four-dimensional (4-D) symbols.

As coded modulation schemes, we investigated BICM<sup>[3]</sup> with uniformly distributed 8, 16, 32, 64, and 128-ary quadrature amplitude modulation (QAM). Probabilistic amplitude shaping<sup>[4]</sup> was also considered, namely PS-16-QAM with symbol entropy  $2\mathbb{H}(X) = 3.4$  bit/channel use (bpcu), PS-64-QAM with  $2\mathbb{H}(X) = 4.1, 4.6, 5.0, 5.2$ , or 5.7 bpcu, and PS-256-QAM with  $2\mathbb{H}(X) = 6.3$  and 7.4 bpcu, where  $\mathbb{H}(\cdot)$  and  $X$  denote entropy and 1-D symbol, respectively. Both BICM and MLC<sup>[8]</sup> were studied. The considered MLC treats only 1-D pulse amplitude modulation symbols. Two lines of 1-D absolute amplitudes for PS-64-QAM having  $2\mathbb{H}(X) = 4.1, 4.6, 5.2$ , or 5.7 were generated by constant composition distribution matching (CCDM)<sup>[16]</sup> with an output block length of 1024 1-D symbols. The amplitudes for the other PS-QAM were given by bit-level PS<sup>[5]</sup> with binary DMs<sup>[17]</sup>.

In both BICM and MLC, virtual FEC coding<sup>[18]</sup> for offline evaluation was assumed using a concatenation of soft-decision (SD) and hard-decision (HD) FEC. The SD-FEC code rate was 4/5 and the FEC threshold was an ASI of 0.86 (5 dB for QPSK)<sup>[19]</sup>. A low redundancy ( $\sim 1\%$ ) HD-FEC with a bit-interleaver cleans up the residual bit errors<sup>[20]</sup>. The SD-FEC in the MLC protects only the least significant bits as information bits. Thus the total FEC redundancy and SD-FEC throughput in MLC were significantly less than that in BICM.

### Results: transceiver SNRs in BICM

To characterize the transceiver SNR, we investigated cases with widely deployed BICM schemes. Fig. 2 shows the estimated transceiver SNR for BICM with (a) uniform QAM and (b) PS-

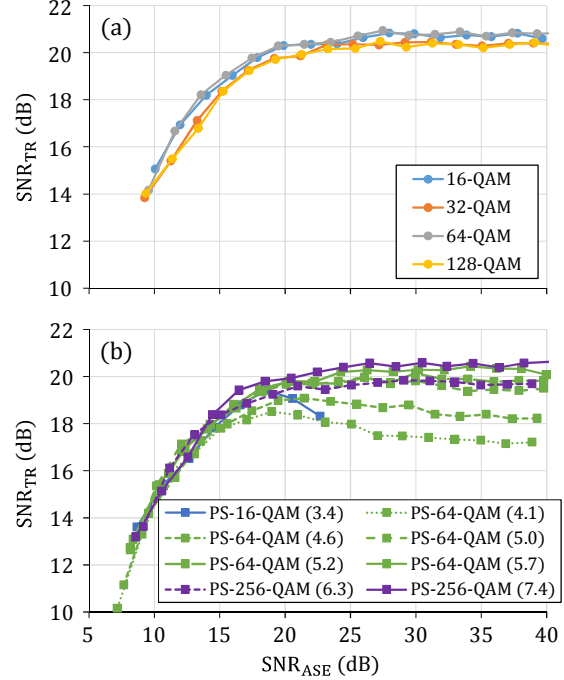


Fig. 2: Transceiver SNR as a function of OSNR for (a) BICM uniform QAM and (b) BICM PS-QAM.

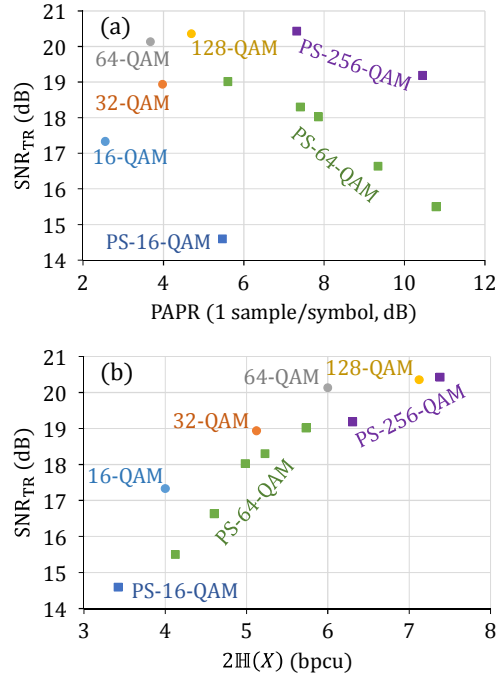


Fig. 3: Transceiver SNR at an FEC threshold as a function of (a) 1-D PAPR or (b) 1-D entropy for BICM uniform QAM (circles) and BICM PS-QAM (squares).

QAM. As a performance metric, we employed ASI. Based on the monitored ASI and SNR-ASI relationship over the ideal Gaussian channels, we derived  $\text{SNR}_{\text{eff}}$ . From the measured OSNR and  $\text{SNR}_{\text{eff}}$ ,  $\text{SNR}_{\text{TR}}$  was obtained based on (1). There are several trends worth noting in Fig. 2. PS-QAMs have smaller  $\text{SNR}_{\text{TR}}$  than uniform QAMs at large enough OSNRs (such as 25–40 dB). The stronger the shaping is, the smaller the

$\text{SNR}_{\text{TR}}$  is for a given base constellation. The  $\text{SNR}_{\text{TR}}$  is less dependent on base constellation or shaping depths but strongly dependent on OSNR when  $\text{OSNR} < 20$  dB. This could be due to inaccuracy of the receiver DSP under such noisy conditions. According to these results, a fixed  $\text{SNR}_{\text{TR}}$  in modeling (defined at a very high OSNR) would fail with a practical transceiver.

Clearly  $\text{SNR}_{\text{TR}}$  around the FEC threshold for error free operation (e.g., ASI = 0.86) is more important than that at large OSNR. Fig. 3 shows  $\text{SNR}_{\text{TR}}$  at the FEC threshold as a function of (a) 1-D PAPR at 1 sample/symbol or (b) symbol entropy  $2\mathbb{H}(X)$  for BICM uniform QAM (circles) and BICM PS-QAM (squares). In Fig. 3(a),  $\text{SNR}_{\text{TR}}$  is smaller for smaller base constellations and larger PAPR (i.e., deeper shaping). In Fig. 3(b),  $\text{SNR}_{\text{TR}}$  depends on  $\mathbb{H}(X)$ , and uniform QAM shows a larger  $\text{SNR}_{\text{TR}}$  than PS-QAM at a given  $\mathbb{H}(X)$ . These behaviors of  $\text{SNR}_{\text{TR}}$  can critically influence the key performance of ROSNR, which we will analyze in the next section.

### Results: ROSNRs in BICM and MLC

ROSNR is the  $\text{SNR}_{\text{ASE}}$  at the FEC threshold, which was derived from the monitored OSNR and the experimental performance (ASI) with the assumed FEC in both the BICM and MLC cases. Fig. 4 shows the ROSNR gap to the Shannon limit and the SNR degradation  $\Delta\text{SNR}$  at the FEC threshold as a function of information rate (IR) for (a) BICM and (b) MLC without DM rate loss<sup>[21]</sup>. The ROSNR reduction by BICM PS-QAM or MLC PS-QAM is significant (1.3–1.4 dB) over uniform 32-QAM but smaller (0.6–0.7 dB) over BICM with uniform 16-QAM. PS-256-QAM shows better performance than BICM with uniform 128-QAM but almost no gain over uniform 64-QAM. Higher-order QAM with a deep shaping (PS-256-QAM with  $2\mathbb{H}(X)$  of 6.3 bpcu) suffers from a smaller  $\text{SNR}_{\text{TR}}$  compared with uniform QAMs, which leads to a larger  $\Delta\text{SNR}$ . Note that  $\Delta\text{SNR}$  is not so close to 0 dB even at  $\text{IR} \approx 2.5$  bpcu, due to a small  $\text{SNR}_{\text{TR}}$  in noisy conditions, as shown in Fig. 2.

Fig. 5 shows the ROSNR gap without and with a DM rate loss of 0.1 bpcu, which is a realistic value for DM implementations for optical fiber communications<sup>[22,23]</sup>. The overall performances of BICM and MLC are similar. At information rates above 4.4 bpcu we see an improvement for MLC over BICM. With a DM rate loss of 0.1 bpcu, MLC PS shows better performance than BICM PS, and entirely beats uniform signalling over the IR range shown in Fig. 5, even with a small transceiver SNR due to PS.

### Conclusions

We experimentally studied SNRs for the coded modulation schemes of BICM, BICM PS, and

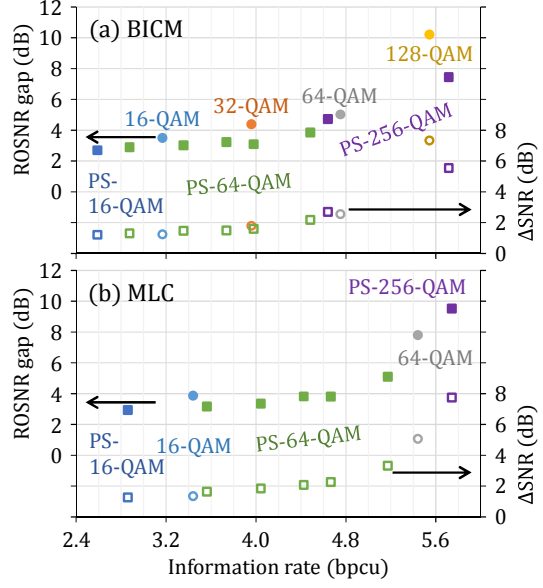


Fig. 4: ROSNR gap to the Shannon limit and  $\Delta\text{SNR}$  as a functions of information rate with several base constellations for (a) BICM and (b) MLC without DM rate loss.

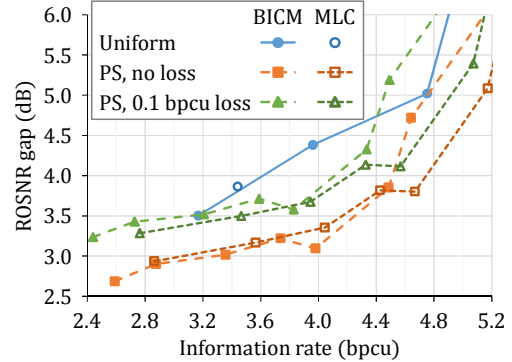


Fig. 5: ROSNR gap to the Shannon limit for BICM and MLC without and with DM rate loss (0.1 bpcu).

MLC PS. The transceiver SNR depends on the OSNR in the low OSNR regime and on the shaping depth in the high OSNR regime, resp. This should be reflected in the deployable system design. Uniform signals show higher transceiver SNR at a given symbol entropy or IR. A significant performance gain by BICM PS or MLC PS over uniform signalling remains in most cases under such a small transceiver SNR if the DM rate loss is within 0.1 bpcu.

### Acknowledgements

This work was partly supported by “Massively Parallel and Sliced Optical Network,” the Commissioned Research of National Institute of Information and Communications Technology (NICT) and “The research and development of innovative optical network technology as a new social infrastructure” of the Ministry of Internal Affairs and Communications, Japan. We thank researchers in NTT and Fujitsu for fruitful discussions. We also thank Prof. Kyo Inoue of Osaka University for assistance in the research.

## References

- [1] G. D. Forney, Jr. and L.-F. Wei, "Multidimensional constellations –Part I: introduction, figure of merit, and generalized cross constellation", *IEEE J. Selected Areas Commun.*, vol. 7, no. 6, pp. 87–892, Aug. 1989.
- [2] F. R. Kschischang and S. Pasupathy, "Optimal nonuniform signaling for Gaussian channels", *IEEE Trans. Inf. Theory*, vol. 39, no. 3, pp. 913–929 , May 1993.
- [3] G. Caire, G. Taricco, and E. Biglieri, "Bit-interleaved coded modulation", *IEEE Trans. Inf. Theory*, vol. 44, no. 3, pp. 927–946, May 1998.
- [4] G. Böcherer, F. Steiner, and P. Schulte, "Bandwidth efficient and rate-matched low-density parity-check coded modulation", *IEEE Trans. Commun.*, vol. 63, no. 12, pp. 4651–4665, Dec. 2015.
- [5] M. Pikus and W. Xu, "Bit-level probabilistically shaped coded modulation", *Commun. Lett.*, vol. 21, no. 9, pp. 1929–1932, Sep. 2017.
- [6] G. Böcherer, P. Schulte, and F. Steiner, "Probabilistic shaping and forward error correction for fiber-optic communication systems", *J. Lightw. Technol.*, vol. 37, no. 2, pp. 230–244, Jan. 2019.
- [7] J. Cho and P. Winzer, "Probabilistic constellation shaping for optical fiber communications", *J. Lightw. Technol.*, vol. 37, no. 6, pp. 1590–1607, Mar. 2019.
- [8] T. Yoshida, M. Karlsson, and E. Agrell, "Multilevel coding with flexible probabilistic shaping for rate-adaptive and low-power optical communications", in *Proc. Opt. Fib. Commun. Conf. (OFC)*, San Diego, CA, USA, Mar. 2020, Paper M3J.7.
- [9] A. Matsushita, M. Nakamura, S. Yamamoto, F. Hamaoka, and Y. Kisaka, "41-Tbps C-band WDM transmission with 10-bps/Hz spectral efficiency using 1-Tbps/λ signals", *J. Lightw. Technol.*, to appear, DOI:10.1109/JLT.2020.2986083, 2020.
- [10] L. Galdino, D. Semrau, D. Lavery, G. Saavedra, C. B. Czegledi, E. Agrell, R. I. Killey, and P. Bayvel, "On the limits of digital back-propagation in the presence of transceiver noise", *Opt. Express*, vol. 25, no. 4, pp. 4564–4578, Feb. 2017.
- [11] G. Kaplan and S. Shamai, "Information rates and error exponents of compound channels with application to antipodal signaling in a fading environment", *Archiv für Elektronik und Übertragungstechnik (AEÜ)*, vol. 47, no. 4, pp. 228–239, 1993.
- [12] T. Yoshida, M. Karlsson, and E. Agrell, "Performance metrics for systems with soft-decision FEC and probabilistic shaping", *Photon. Technol. Lett.*, vol. 29, no. 23, pp. 2111–2114, Dec. 2017.
- [13] T. Yoshida, A. Alvarado, M. Karlsson, and E. Agrell, "Post-FEC BER benchmarking for bit-interleaved coded modulation with probabilistic shaping", *J. Lightw. Technol.*, vol. 38, no. 16, pp. 4292–4306, August 2020.
- [14] T. Yoshida, M. Mazur, J. Schröder, M. Karlsson, and E. Agrell, "Performance monitoring for live systems with soft FEC and multilevel modulation", *J. Lightw. Technol.*, vol. 38, no. 11, pp. 2912–2921, June 2020.
- [15] M. Mazur, J. Schröder, A. Lorences-Riesgo, T. Yoshida, M. Karlsson, and P. A. Andrekson, "Overhead optimization of pilot-based digital signal processing for flexible high spectral efficiency transmission", *Opt. Express*, vol. 27, no. 17, pp. 24654–24669, Aug. 2019.
- [16] P. Schulte and G. Böcherer, "Constant composition distribution matching", *IEEE Trans. Inf. Theory*, vol. 62, no. 1, pp. 430–434, Jan. 2016.
- [17] T. Yoshida, M. Karlsson, and E. Agrell, "Low-complexity variable-length output distribution matching with periodical distribution uniformization", in *Proc. Opt. Fib. Commun. Conf. (OFC)*, San Diego, CA, USA, Mar. 2018, Paper M4E.2.
- [18] T. Yoshida, M. Karlsson, and E. Agrell, "Efficient offline evaluation of FEC codes based on captured data with probabilistic shaping", in *Proc. Opt. Fib. Commun. Conf. (OFC)*, San Diego, CA, USA, Mar. 2018, Paper M4E.5.
- [19] K. Sugihara, Y. Miyata, T. Sugihara, K. Kubo, H. Yoshida, W. Matsumoto, and T. Mizuochi, "A spatially-coupled type LDPC code with an NCG of 12 dB for optical transmission beyond 100 Gb/s", in *Proc. Opt. Fib. Commun. Conf. (OFC)*, Anaheim, CA, USA, Mar. 2013, Paper OM2B.4.
- [20] D. S. Millar, R. Maher, D. Lavery, T. Koike-Akino, M. Pajovic, A. Alvarado, M. Paskov, K. Kojima, K. Parsons, B. C. Thomsen, S. Savory, and P. Bayvel, "Detection of a 1 Tb/s superchannel with a single coherent receiver," in *Proc. Eur. Conf. Opt. Commun. (ECOC)*, Valencia, Spain, Sep. 2015, Paper Mo.3.3.1.
- [21] T. Fehenberger, D. S. Millar, T. Koike-Akino, K. Kojima, and K. Parsons, "Multiset–partition distribution matching", *IEEE Trans. Commun.*, vol. 67, no. 3, pp. 1885–1893, Mar. 2018.
- [22] T. Yoshida, M. Karlsson, and E. Agrell, "Hierarchical distribution matching for probabilistically shaped coded modulation", *J. Lightw. Technol.*, vol. 37, no. 6, pp. 1579–1589, Mar. 2019.
- [23] T. Yoshida, M. Binkai, S. Koshikawa, S. Chikamori, K. Matsuda, N. Suzuki, M. Karlsson, and E. Agrell, "FPGA implementation of distribution matching and dematching", in *Proc. Eur. Conf. Opt. Commun. (ECOC)*, Dublin, Ireland, Sep. 2019, Paper M.2.D.2.